Inorganic Chemistry

pubs.acs.org/IC Article

{$P_2V_3W_{15}$}-Polyoxometalates Functionalized with Phthalocyaninato Y and Yb Moieties

Ricarda Pütt, Piotr Kozłowski, Irina Werner, Jan Griebel, Sebastian Schmitz, Jonas Warneke, and Kirill Yu. Monakhov*

Cite This: https://dx.doi.org/10.1021/acs.inorgchem.0c02257 Read Online

ACCESS | Metrics & More | Article Recommendations | Supporting Information

ABSTRACT: A tris(alkoxo)pyridine-augmented Wells–Dawson polyoxometalate (nBu$_4$N)$_6$[**WD-Py**] (WD = $P_2V_3W_{15}O_{59}(OCH_2)_3C$, Py = C_5H_4N) was functionalized with phthalocyaninato metal moieties (**MPc** where M = Y or Yb and Pc = $C_{32}H_{16}N_8$) to afford (nBu$_4$N)$_4$[H**WD-Py**(**MPc**)] compounds. High-resolution mass spectrometry was used to detect and identify the hybrid assembly. The magnetism studies reveal substantial differences between M = Yb (monomeric, single-ion paramagnetism) and M = Y (containing dimers, radical character). The results of electronic paramagnetic resonance spectroscopy, SQUID magnetometry, and magnetochemical calculations indicate the presence of *intra*molecular charge transfer from the **MPc** moiety to the polyoxometalate and of *inter*molecular charge transfer from the **MPc** moiety of one molecule to the polyoxometalate unit of another molecule. These compounds with identified V^{IV} ions represent unique examples of transition-metal/lanthanide complex-POM hybrid compounds with nonphotoinduced charge transfer between electron donor and acceptor centers.

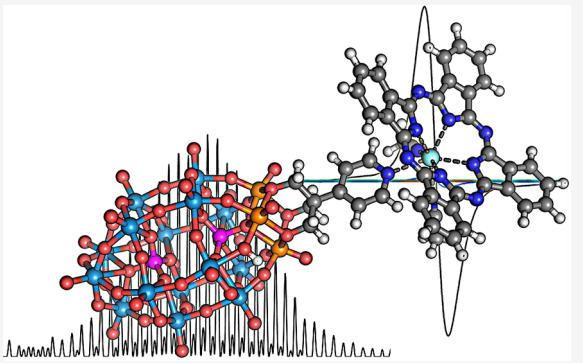

1. INTRODUCTION

Polyoxometalate (POM)-based organic–inorganic hybrid compounds constitute a large part of stimuli-responsive materials with promising applications in photo/electrocatalysis, molecular magnetism, and energy storage.[1−13] In particular, their development is pursued due to high interest for photoinduced charge transfer between transition-metal/lanthanide complex units and POM. The effective attachment of the former to the polyoxoanion unit can be effectively realized via organic functional groups and linkages, which are structurally exposed at the molecular periphery of POM through well-established functionalization and postfunctionalization mechanisms.[2,3,14−16] For instance, the formation of the molecular heterometal metal-to-POM charge transfer (MPCT) chromophore with a short-lived charge-separated state has been observed in the compound $K_{15}NaP_4W_{35}O_{124}\{Re(CO)_3\}_2\cdot 37H_2O$ and its organic-solvent-soluble analog (nBu$_4$N)$_{15}$[$HP_4W_{35}O_{124}$]{$Re(CO)_3$}$_2\cdot 0.3CH_2Cl_2$, which consist of a $[Re(CO)_3]^+$ unit bound directly to the lacunary Wells–Dawson-type POM $[\alpha_2\text{-}P_2W_{17}O_{61}]^{10-}$.[17] Photoinduced long-lived charge-separated states were reported for the photosensitizer-POM hybrids separated by a π-conjugated spacer; examples include Ru(II)-bis(terpyridine)- or Ru(II)-(tpy)$_2$[$PW_{11}O_{39}Ge$]$^{4-}$ (Keggin-type),[18,19] related cyclometalated Ir(III) complexes-POMs (Keggin- or Wells–Dawson-type),[20] and noble metal-free bodipy fluorophores linked to Si- or Sn-functionalized Keggin-type POMs.[21] A through-space mechanism of electron charge transfer was described for tris(alkoxo)-Csp^3-derivatized POMs (a Wells–Dawson-type $[P_2V_3W_{15}O_{62}]^{9-}$ or an Anderson-type POM) linked by a bipyridine group to Re(I)-,[21,22] Rh(III)-, and Ir(III)-complexes[23,24] or by an amido functionality to the Zn(II) tetraphenylporphyrin complex.[25] Advances in the area of charge-transfer materials based on photosensitizer-POMs hybrid assemblies are comprehensively discusssed in the reviews by Santoni[26] and Keyes.[27]

The above-mentioned findings came to our attention, triggering the exploration of charge-transfer states in electron donor–acceptor transition-metal/lanthanide complex-POM hybrid compounds for their application and controlled modification on electrode surfaces.[28] Recent studies in the field of molecular electronics have shown that POM-based organic–inorganic hybrids can adsorb, for example, on gold substrates as intact single molecules or in the form of self-assembled monolayers (SAMs), and their electronic states can be changed multiple times by electrical means.[29−31] It is therefore worth investigating POMs[9,32−34] with their appealing

Received: July 29, 2020

electron transport characteristics as individual molecules and in conjunction with transition-metal/lanthanide complexes for molecule-based "More than Moore" information technology.[35]

The latest developments in the areas of POM-based charge-transfer and POM-on-a-surface materials have prompted us to elaborate (post)functionalization approaches[16,36] toward the formation of hybrid assembly where POM is connected directly or via an organic linker to a metal ion ligated by the redox-active phthalocyanine (Pc) ligand.[37] Several of these studies are ongoing to assess, on the one hand, the ability of the target hybrid compounds to exhibit electron donor−acceptor structures with ground-state charge transfer and to unveil, on the other hand, their adsorption site preferences on surfaces. In this regard, we could already showcase the direct coordination of phthalocyaninato Yb^{III} moieties onto the fully oxidized, lacunary $\{V_{12}O_{32}\}$-type polyoxovanadate cage and the generation of conductive SAMs made of these hybrid complexes on gold surfaces.[30]

In the present study we focus on the connection of phthalocyaninato Y^{III}/Yb^{III} (= M) moieties to POM via an organic linker (Figure 1). We have succeeded in the formation

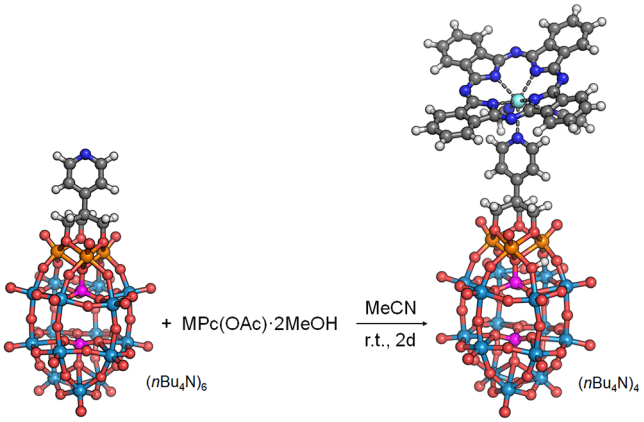

Figure 1. Synthesis of the $(n\mathrm{Bu_4N})_4[\mathrm{HWD\text{-}Py(MPc)}]$ compounds with M = Y and Yb from the $(n\mathrm{Bu_4N})_6[\mathbf{WD\text{-}Py}]$ and MPc(OAc) precursors in MeCN. The H^+ proton of the POM is not shown. r.t. = room temperature. Color code: M = cyan, W = light blue, V = orange, O = red, N = dark blue, P = purple, C = gray, H = white. See the SI for details of synthesis, analytical characterization, and crystallographic data.

of two hybrid assemblies $(n\mathrm{Bu_4N})_4[\mathrm{HP_2V_3W_{15}O_{59}(OCH_2)_3CC_5H_4N)(C_{32}H_{16}N_8M)}]$ (hereafter referred to as $(n\mathrm{Bu_4N})_4[\mathrm{HWD\text{-}Py(MPc)}]$) that feature different magnetic characteristics depending on the type of a phthalocyaninato metal moiety ($\mathbf{MPc}^+$) attached at the periphery of the organically modified Wells−Dawson-type polyoxoanion $[\mathrm{HP_2V_3W_{15}O_{59}(OCH_2)_3CC_5H_4N}]^{5-}$ (= $\{\mathrm{HWD\text{-}Py}\}^{5-}$) . The synthesized compounds were characterized by various methods, including electrospray ionization mass spectrometry (ESI-MS), electron paramagnetic resonance (EPR) spectroscopy, and magnetic susceptibility measurements combined with magnetochemical calculations. This thus continues the series of our works about the synthesis and properties of POMs functionalized with phthalocyaninato lanthanide moieties and about the behavior and performance of tris(alkoxo)-ligated Wells−Dawson-type POM surfactants, such as $\{[\mathrm{HP_2V^V_3W^{VI}_{15}O_{59}((OCH_2)_3CCH_2OCH_2C_6H_4I)]}\}^{5-}$, in discrete solutions and on surfaces.[38]

2. RESULTS AND DISCUSSION

2.1. Synthesis and Structure Characterization. The pyridine-containing triol-ligand $(\mathrm{HOCH_2})_3\mathrm{CC_5H_4N}$ was obtained by the reaction of 4-methylpyridine and an aqueous formaldehyde solution at 100 °C in an autoclave, according to the literature procedure.[39] The reaction of $(\mathrm{HOCH_2})_3\mathrm{CC_5H_4N}$ with the POM $(n\mathrm{Bu_4N})_5[\mathrm{H_4P_2V_3W_{15}O_{62}}]$[40] in a 1:1 ratio at 85 °C in MeCN yielded a trisalkoxo-derivatized $(n\mathrm{Bu_4N})_6[\mathbf{WD\text{-}Py}]$ compound with the pyridine (Py) group at the molecular periphery. The composition (including the number of $n\mathrm{Bu_4N^+}$ (= $(\mathrm{C_4H_9})_4\mathrm{N^+}$) countercations) and the structural integrity of $(n\mathrm{Bu_4N})_6[\mathbf{WD\text{-}Py}]$ were determined by CHN elemental analysis (see Table S1), ^{1}H-, ^{31}P-, and ^{51}V-NMR and IR spectroscopy (see Figure S1). The NMR spectra show one ^{51}V signal at −544 ppm and two ^{31}P signals at −7.54 and −13.67 ppm, thus corroborating the absence of isomeric Wells−Dawson-type species. Also, the ^{1}H NMR spectra show characteristic signals from the Py protons at δ = 8.61 and 7.51 ppm and from the six $-CH_2$ protons of the trisalkoxo ligand as a singlet at 5.61 ppm.

The follow-up room temperature (r.t.) reaction of $(n\mathrm{Bu_4N})_6[\mathbf{WD\text{-}Py}]$ with heteroleptic MPc(OAc)·2MeOH (PcOAc = $\mathrm{C_{34}H_{19}N_8O_2}$) in a 1:1 ratio in MeCN and the workup with Et_2O resulted in the trimetallic compounds $(n\mathrm{Bu_4N})_4[\mathrm{HWD\text{-}Py(MPc)}]\cdot 2\mathrm{Et_2O}$, where the peripheral Py group of the inorganic−organic $(n\mathrm{Bu_4N})_6[\mathbf{WD\text{-}Py}]$ hybrid is axially connected to the **MPc** moiety (Figure 1). Their elemental composition analysis (Table S1) indicates the presence of four $n\mathrm{Bu_4N^+}$ counterions, one proton at the POM unit, and two Et_2O units as co-crystallized solvent molecules. Thermogravimetric data (Table S2) are in line with elemental analysis. The compounds show thermal stability up to ca. 220 °C in air and ca. 260 °C under nitrogen. The loss of the diethyl ether solvent molecules was observed for each analyzed compound.

The IR spectra of $(n\mathrm{Bu_4N})_5[\mathbf{WD}]$, $(n\mathrm{Bu_4N})_6[\mathbf{WD\text{-}Py}]$, $(n\mathrm{Bu_4N})_4[\mathrm{HWD\text{-}Py(YPc)}]$, and $(n\mathrm{Bu_4N})_4[\mathrm{HWD\text{-}Py(YbPc)}]$ are characterized by O—P—O, V═O, W═O, and O—W—O vibrations in the 1100−700 cm^{-1} region, which are typical for these Wells−Dawson-type POMs.[40,41] No significant difference between the IR spectra of the pyridine-containing POMs $[\mathbf{WD\text{-}Py}]^{6-}$ and $[\mathrm{HWD\text{-}Py(MPc)}]^{4-}$ was observed for the C—N—C vibration of the pyridine moiety, which appears each as a weak absorption band at around 1595 cm^{-1}. In addition, the $[\mathrm{HWD\text{-}Py(MPc)}]^{4-}$ hybrids show characteristic CH deformation vibrations at 1400−1100 cm^{-1} assigned to the Pc group.[42] A more detailed comparison of the IR spectra of the respective compounds can be found in Figure S1.

^{1}H, ^{31}P, and ^{51}V NMR spectroscopy measurements (see spectra in the SI) were performed only for $(n\mathrm{Bu_4N})_4[\mathrm{HWD\text{-}Py(YPc)}]$ with the diamagnetic character of yttrium. Compared to the ^{1}H NMR spectrum of $(n\mathrm{Bu_4N})_6[\mathbf{WD\text{-}Py}]$, no shift in peak position of $-CH_2$ protons of the trisalkoxo ligand in the title compound is observed. The protons of the Py ring, however, are slightly shifted upfield, which points out the changes in the coordination environment of Py with the protons in the meta position being most affected ($\Delta\delta$ = ca. 0.1 ppm). The ^{31}P (δ = −7.59 and −13.73 ppm) and ^{51}V NMR (δ = −543 ppm) spectra are characterized by a minor

https://dx.doi.org/10.1021/acs.inorgchem.0c02257
Inorg. Chem. XXXX, XXX, XXX−XXX

shift of the respective nuclei compared to those of $(n\mathrm{Bu_4N})_6$[**WD-Py**].

The presence of the phthalocyanine ligand in the title compounds $(n\mathrm{Bu_4N})_4$[H**WD-Py(MPc)**] with M = Y or Yb is evident from their UV/vis spectra (see Figure S2), illustrating characteristic absorption bands,[42,43] i.e., a broad one at ca. 333 nm (*B* band) and an intense one at ca. 680 nm (*Q* band). These bands are shifted by ca. 10 nm with respect to those of the MPc(OAc)·2MeOH precursors. The absorption bands in the wavelength range of 200−300 nm displayed by both $(n\mathrm{Bu_4N})_4$[H**WD-Py(MPc)**] compounds reflect, in particular, ligand-to-metal charge transfer within the POM core (O to W/V) and metal-to-ligand charge transfer between the Y/Yb and Pc units.

The formation of the title coordination compounds is also strongly supported by the signals with broad isotopic patterns found in high-resolution ESI mass spectra (Figure 2, see also Figures S3 and S4). Although we could observe signals indicating a dissociation of the hybrid assembly in solution, the most intense signals can be clearly attributed to the title compounds. The small signals clearly visible between the signals of POM-based ions $\{(n\mathrm{Bu_4N})$[**WD-Py(YPc)**]$\}^{4-}$ (Figure 2a) point out the presence of a dimeric species (with double mass and double charge). Thus, strong intermolecular forces are necessary to hinder dimers of high charge states from fragmentation in the gas phase. Corresponding signals are, however, absent in the case of the $\{(n\mathrm{Bu_4N})_2$[**WD-Py(YbPc)**]$\}^{3-}$ ions (Figure 2b) or any other detected combination of [**WD-Py(YbPc)**]$^{5-}$ with counterions. Therefore, no dimers were found when M is Yb.

2.2. EPR Spectral Characteristics. The room temperature EPR measurements of the title $(n\mathrm{Bu_4N})_4$[H**WD-Py(MPc)**] compounds in MeCN revealed no signal for the species with M = Yb and a signal for M = Y (Figure 3). The latter was found to match to a free delocalized organic radical[44] with a *g* value of 2.0014 and a line width ΔB_{pp} = 0.7 mT.

The monitoring of the room temperature EPR spectra of the $(n\mathrm{Bu_4N})_4$[H**WD-Py(YPc)**] compound at three different concentrations (*c* = 5.0, 1.0, and 0.1 mM) in MeCN solution revealed an intense signal at the highest concentration and a very weak to no signal in low-concentrated solutions. At the 0.1 mM concentration in the measured 20 μL of solution the number of spins is calculated to be 10^{15}, which is still within a detectable range of spin concentration according to the literature 10^{14} spins.[45] This might indicate that the detected EPR signal enhancement takes place when the $(n\mathrm{Bu_4N})_4$[H**WD-Py(YPc)**] species get in closer proximity to each other due to a higher concentrated solution. Thus, it models to some extent a situation in the solid state where the electron transfer is likely to occur between the neighboring {H**WD-Py(YPc)**} units.

The solid-state EPR spectra of $(n\mathrm{Bu_4N})_4$[H**WD-Py(MPc)**] measured at 77 K showed in both cases (Figure 4), beside a radical character of the compound with M = Y, an additional hyperfine structure typical for isolated VO^{2+} ions with the following values of *g* and *A* tensors: $g_\perp$ = 1.9675, $g_\parallel$ = 1.9125, $A_\perp$ = 61.5 G, and $A_\parallel$ = 188.0 G. This hyperfine structure points to the reduction of one of the V^V ions in the POM to the magnetically active V^{IV}. The corresponding EPR measurements of $(n\mathrm{Bu_4N})_4$[H**WD-Py(MPc)**] at r.t. gave the same results with lower intensity of V^{IV} signals, though. The precursor $NaVO_3$, the only vanadium source in the synthesis of $(n\mathrm{Bu_4N})_5$[**WD**], is EPR silent.

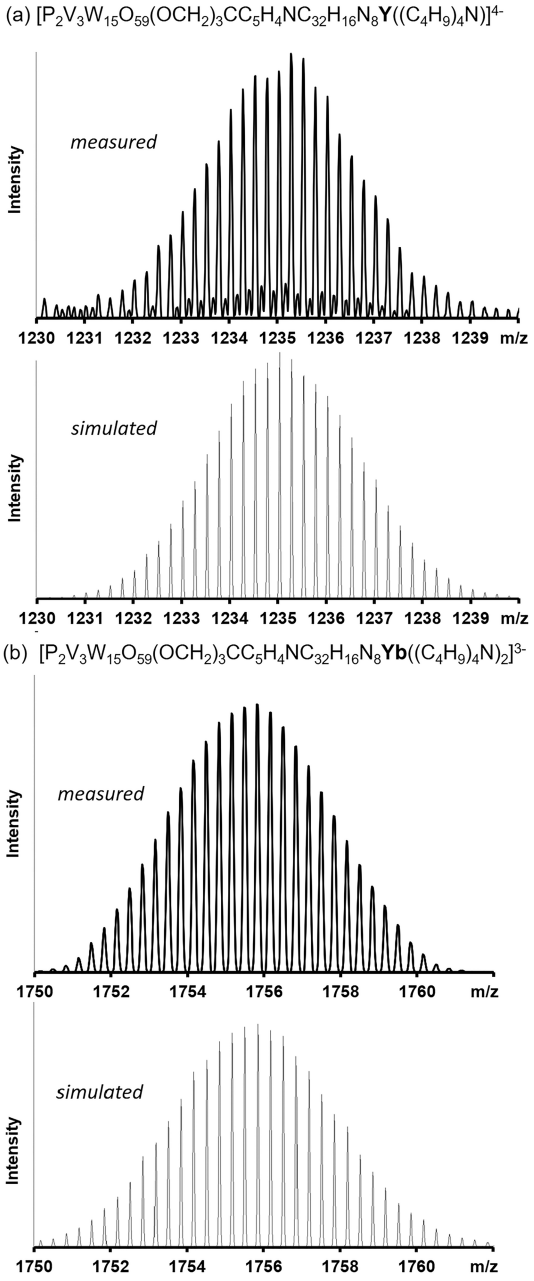

Figure 2. Measured and simulated isotopic patterns of fragments $[P_2V_3W_{15}O_{59}(OCH_2)_3CC_5H_4NC_{32}H_{16}N_8Y((C_4H_9)_4N)]^{4-}$ (a) and $[P_2V_3W_{15}O_{59}$-$(OCH_2)_3CC_5H_4NC_{32}H_{16}N_8Yb((C_4H_9)_4N)_2]^{3-}$ (b) in the negative ion-mode obtained from ESI-MS experiments with the $(n\mathrm{Bu_4N})_4$[H**WD-Py(MPc)**] compounds (M = Y and Yb) in MeCN. See the SI for more details.

The room temperature solid-state EPR spectra of the MPc(OAc) complexes exhibit a radical signal for M = Y and no signal for M = Yb. This is quite interesting since a similar compound $[YPc_2]^-$ containing YPc^+ moiety has no radical character,[46] contrary to the neutral compound YPc_2[47] containing YPc^{2+} moiety. The radical character of metal monophthalocyanine complexes was first described by Sugimoto et al. for MPc(dpm)$_2$ complexes (dpm = tris-(2,2,6,6-tetramethyl-3,5-heptanedionato; M = Lu, Y).[48] The authors observed characteristic EPR signals at r.t. in both the solid state and solution, with a *g* value of 2.001. The EPR spectra had similar shapes and *g* values for stable metal-free

https://dx.doi.org/10.1021/acs.inorgchem.0c02257
Inorg. Chem. XXXX, XXX, XXX−XXX

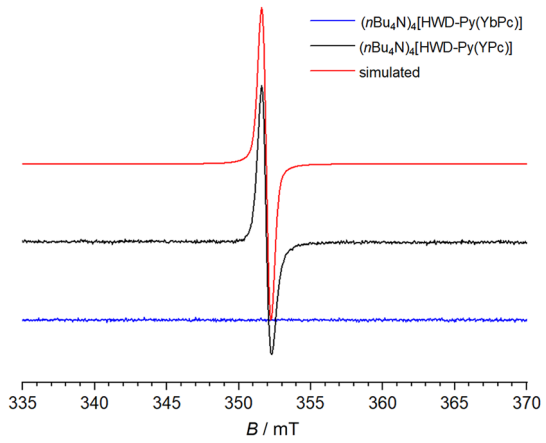

Figure 3. Solution EPR spectra of $(n\mathrm{Bu_4N})_4$[**HWD-Py(MPc)**] (c = 1.2 mM, MeCN) measured at r.t. at a frequency of 9.86 GHz, modulation amplitude of 0.1 mT, and microwave power of 0.2 mW. Color code: M = Yb, blue; M = Y, black; a simulated spectrum, red.

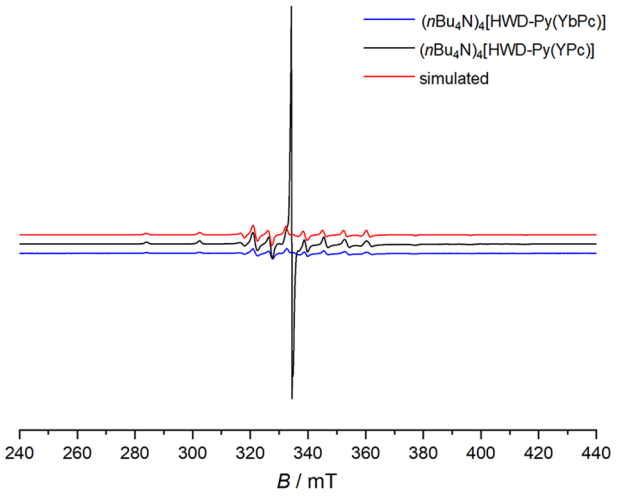

Figure 4. Solid-state EPR spectra of $(n\mathrm{Bu_4N})_4$[**HWD-Py(MPc)**] measured at 77 K at a frequency of 9.44 GHz, modulation amplitude of 0.1 mT, microwave power of 0.2 mW, and T = 77 K. Color code: M = Yb, blue; M = Y, black; a simulated spectrum, red.

[H(Pc$^-$)] and lithiated phthalocyanine [Li(Pc$^-$)] radicals,[49,50] generated by a chemical or electrochemical oxidation. Recently, Reecht et al. showed that in HPc radical the dangling σ bond after N−H cleavage is filled by an electron from the delocalized HOMO via intramolecular charge transfer, providing for a delocalized radical state.[51]

2.3. Magnetic Susceptibility and Magnetochemical Characteristics. Next, magnetic properties of the title $(n\mathrm{Bu_4N})_4$[**HWD-Py(MPc)**] compounds were assessed by standard SQUID technique (0.1−5.0 T and 2.0−290 K) in combination with effective Hamiltonian calculations. For M = Yb the interpretation of the results is rather straightforward. The lack of strong EPR signal at room temperature and the expected +III oxidation state of Yb indicate that the magnetism of this compound should originate mostly from the Yb^{III} ion. The EPR signal of rare earth ions can be obtained only in low (liquid helium) temperatures.[52] Like in the case of related $\{[V_{12}O_{32}(Cl)](LnPc)_n\}^{n-5}$ compounds with n = 1 or 2 and Ln = Yb^{III},[30] we assume that only the ground multiplet with a total angular momentum J = 7/2 arising from spin−orbit coupling is relevant for modeling the magnetism below room temperature. The best fit of the experimental data was obtained with the Hamiltonian:

$$H = -\mu_B g_\perp (J_x B_x + J_y B_y) - \mu_B g_\parallel J_z B_z + D J_z^2 \quad (1)$$

where $J = (J_x, J_y, J_z)$ (J = 7/2) is a total angular momentum, B is the magnetic field, and the parameters assume the anisotropic g-factors of $g_\perp$ = 1.063 and $g_\parallel$ = 1.907 and the anisotropy D/k_B = 96.2 K. In Figure 5 the molar susceptibility and magnetization of $(n\mathrm{Bu_4N})_4$[**HWD-Py(YbPc)**] are shown together with the theoretical curves. The details of the modeling can be found in the SI.

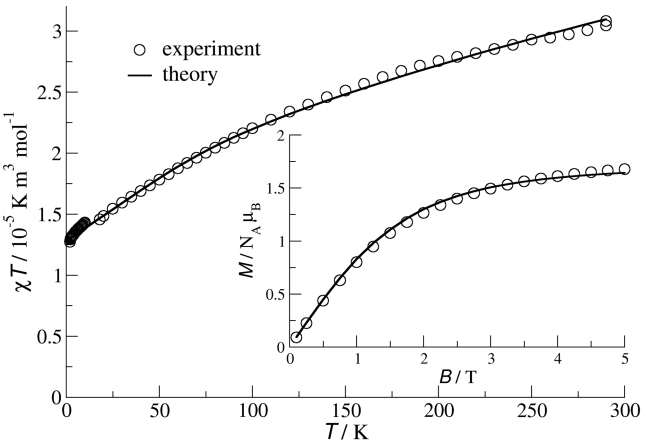

Figure 5. Molar susceptibility (B = 0.1 T) and magnetization (T = 2 K) for $(n\mathrm{Bu_4N})_4$[**HWD-Py(YbPc)**] (circles) with theoretical fits (solid lines).

For the Y^{III}-containing POM-based hybrid assembly the situation is more complicated (Figure 6). The appearance of the EPR signal with the increase of compound concentration may indicate that the proximity of the molecules leads to some change in the magnetism, caused for example by the electron transfer. This conjecture is additionally confirmed by ESI mass spectrometry showing the presence of dimers (see Figure 2).

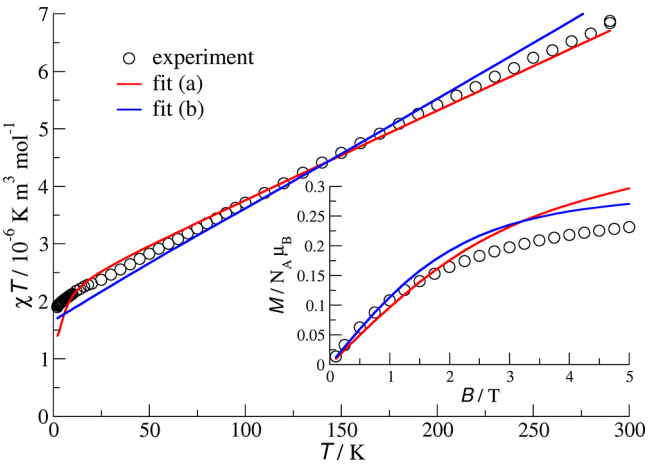

Figure 6. Molar susceptibility (B = 0.1 T) and magnetization (T = 2 K) for $(n\mathrm{Bu_4N})_4$[**HWD-Py(YPc)**] (circles) with theoretical fits (solid lines).

https://dx.doi.org/10.1021/acs.inorgchem.0c02257
Inorg. Chem. XXXX, XXX, XXX−XXX

To account for the results of EPR and ESI-MS it is assumed that some *inter-* and *intra*molecular electron transfer takes place. For instance, an electron from Pc^{2-} may jump to another molecule. In this way two ions $[HWD\text{-}Py(YPc)]^{3-}$ and $[HWD\text{-}Py(YPc)]^{5-}$ are formed. Each of these ions has now one unpaired electron. The first one is likely located at Pc^{-}; the other, for example, may reduce V^{V} to V^{IV}, as supported by the hyperfine structure in the solid-state EPR spectrum at low temperature, or it may be delocalized over a bigger part of the molecule. An *intra*molecular electron transfer apparently occurs from Pc^{2-} to POM, giving as a result a molecule with two unpaired electrons. However, these mechanisms, even if they coexist, are not able to explain the linear increase of χT with temperature. Such a behavior suggests either strong antiferromagnetic interaction (or anisotropy) or the presence of temperature independent paramagnetism (TIP). Notably, both mechanisms are observed in similar compounds with a linear dependence of χT on temperature. For instance, in a molecular compound $[K(18\text{-crown-}6)(THF)_2][(Cp''_2La)_2\text{-}(\mu{-}\eta^6{:}\eta^6\text{-}C_6H_6)]\cdot THF$ containing La^{II} ions[53] any of these two mechanisms could be used to account for linear dependence of χT on temperature. In $[K(2.2.2\text{-cryptand})][Cp'_3Y]$ containing a Y^{II} ion the linear dependence of χT on temperature was attributed to TIP.[54] Therefore, in the magnetic modeling we assumed that a fraction p_1 of the molecules contains one unpaired electron and a fraction p_2 contains two unpaired electrons possibly interacting with strength K. In addition, we assume the presence of TIP. The fitting of the susceptibility and magnetization leads to the conclusion that to account for the linear increase of χT with temperature the TIP contribution is indispensable. The introduction of interaction between the unpaired electrons located at one molecule can improve fitting of magnetization.

Figure 6 illustrates the results of two optimal fits. In fit (a), $p_1 = 0.29$ and $p_2 = 0.094$ and the interaction is antiferromagnetic ($K/k_B = 11.8$ K). Susceptibility induced by TIP is estimated to be equal to $\chi_{TIP} = 1.53 \times 10^{-8}$ m^3 mol^{-1}. The remaining fraction $p_3 = 0.62$ of the molecules is not magnetically active. This result can also be interpreted in this way that the molecules with one unpaired electron are parts of dimers in which an electron transfer took place, whereas those with two unpaired electrons appear as a result of *intra*molecular electron transfer. In fit (b), $p_1 = 0.0006$ and $p_2 = 0.13$ and the interaction is ferromagnetic ($K/k_B = -217$ K). Susceptibility induced by TIP is estimated to be equal to $\chi_{TIP} = 2.01 \times 10^{-8}$ m^3 mol^{-1}. The remaining fraction $p_3 = 0.87$ of the molecules is not magnetically active. Both fits reproduce a general character of the susceptibility and magnetization curves depicted in Figure 6 but are far from ideal. It strongly suggests that an improved magnetochemical model[55−57] needs to be further fine-tuned for such intricate electronic situations described herein, work that is currently in progress. The determination of the precise source of TIP is also needed. More details on modeling the magnetism of $(n\text{Bu}_4\text{N})_4[HWD\text{-}Py(YPc)]$ can be found in the SI.

3. CONCLUSIONS

The Wells−Dawson $P_2V_3W_{15}$-type POM with the structurally exposed tris(alkoxo)pyridine functionality provided a connection to phthalocyaninato Y and Yb moieties. The spectroscopic and magnetic measurements indicated that the interaction of MPc units with the fully oxidized POM-based organic−inorganic hybrid gives rise to a donor−acceptor structure and a radical character for M = Y and a single-ion paramagnetic character for M = Yb. Femtosecond transient absorption spectroscopy and pulse radiolysis experiments accompanied by quantum mechanical calculations are currently in progress to gain deeper insights into the mechanism of the observed *intra-* and *inter*molecular electron charge transfer from MPc to the $\{V_3\}$ triad of POM ($V^{V} \rightarrow V^{IV}$) and into underlying changes in the electronic structure. The findings described herein are especially of high interest for studies of radical spin effects on electron transport characteristics of POM compounds, their molecular ordering, and electron communication on surfaces.

■ ASSOCIATED CONTENT

Supporting Information

The Supporting Information is available free of charge at https://pubs.acs.org/doi/10.1021/acs.inorgchem.0c02257.

Details of synthesis, analytical characterization, and magnetism (PDF)

■ AUTHOR INFORMATION

Corresponding Author

Kirill Yu. Monakhov − *Leibniz Institute of Surface Engineering (IOM), 04318 Leipzig, Germany;* orcid.org/0000-0002-1013-0680; Email: kirill.monakhov@iom-leipzig.de

Authors

Ricarda Pütt − *Institute of Inorganic Chemistry, RWTH Aachen University, 52074 Aachen, Germany*

Piotr Kozłowski − *Faculty of Physics, Adam Mickiewicz University in Poznań, 61-614 Poznań, Poland*

Irina Werner − *Leibniz Institute of Surface Engineering (IOM), 04318 Leipzig, Germany*

Jan Griebel − *Leibniz Institute of Surface Engineering (IOM), 04318 Leipzig, Germany*

Sebastian Schmitz − *Leibniz Institute of Surface Engineering (IOM), 04318 Leipzig, Germany*

Jonas Warneke − *Leibniz Institute of Surface Engineering (IOM), 04318 Leipzig, Germany; Wilhelm-Ostwald-Institute for Physical and Theoretical Chemistry, Leipzig University, 04103 Leipzig, Germany*

Complete contact information is available at: https://pubs.acs.org/10.1021/acs.inorgchem.0c02257

Notes

The authors declare no competing financial interest.

■ ACKNOWLEDGMENTS

This work was supported by the Emmy Noether program and Individual Research Grant (project no. 432224404) of the Deutsche Forschungsgemeinschaft (DFG). Computational time from the ZIH Dresden is gratefully acknowledged. Some model Hamiltonian calculations were carried out at the Poznań Supercomputing and Networking Centre in Poland. J.W. acknowledges a Freigeist Fellowship of the Volkswagen Foundation. The authors thank Prof. Bernd Abel (Leipzig University, IOM) for access to an LTQ Orbitrap XL and Dr. Jan van Leusen (RWTH Aachen University) for helpful discussions on magnetism.

https://dx.doi.org/10.1021/acs.inorgchem.0c02257
Inorg. Chem. XXXX, XXX, XXX−XXX

REFERENCES

(1) Pradeep, C. P.; Long, D.-L.; Newton, G. N.; Song, Y.-F.; Cronin, L. Supramolecular metal oxides: Programmed hierarchical assembly of a protein-sized 21 kDa $[(C_{16}H_{36}N)_{19}\{H_2NC(CH_2O)_3P_2V_3W_{15}O_{59}\}_4]^{5-}$ polyoxometalate assembly. *Angew. Chem., Int. Ed.* **2008**, *47*, 4388−4391.

(2) Dolbecq, A.; Dumas, E.; Mayer, C. R.; Mialane, P. Hybrid organic-inorganic polyoxometalate compounds: From structural diversity to applications. *Chem. Rev.* **2010**, *110*, 6009−6048.

(3) Proust, A.; Matt, B.; Villanneau, R.; Guillemot, G.; Gouzerh, P.; Izzet, G. Functionalization and post-functionalization: a step towards polyoxometalate-based materials. *Chem. Soc. Rev.* **2012**, *41*, 7605−7622.

(4) Santoni, M.-P.; Hanan, G. S.; Hasenknopf, B. Covalent multicomponent systems of polyoxometalates and metal complexes: Toward multi-functional organic−inorganic hybrids in molecular and material sciences. *Coord. Chem. Rev.* **2014**, *281*, 64−85.

(5) Walsh, J. J.; Bond, A. M.; Forster, R. J.; Keyes, T. E. Hybrid polyoxometalate materials for photo(electro-) chemical applications. *Coord. Chem. Rev.* **2016**, *306*, 217−234.

(6) Li, X.-X.; Wang, Y.-X.; Wang, R.-H.; Cui, C.-Y.; Tian, C.-B.; Yang, G.-Y. Designed assembly of heterometallic cluster organic frameworks based on Anderson-type polyoxometalate clusters. *Angew. Chem., Int. Ed.* **2016**, *55*, 6462−6466.

(7) Yazigi, F.-J.; Wilson, C.; Long, D.-L.; Forgan, R. S. Synthetic considerations in the self-assembly of coordination polymers of pyridine-functionalised hybrid Mn-Anderson polyoxometalates. *Cryst. Growth Des.* **2017**, *17*, 4739−4748.

(8) Cameron, J. M.; Wales, D. J.; Newton, G. N. Shining a light on the photo-sensitisation of organic-inorganic hybrid polyoxometalates. *Dalton Trans.* **2018**, *47*, 5120−5136.

(9) Stuckart, M.; Monakhov, K. Y. Polyoxometalates as components of supramolecular assemblies. *Chem. Sci.* **2019**, *10*, 4364−4376.

(10) Amin, S.; Cameron, J. M.; Watts, J. A.; Walsh, D. A.; Sans, V.; Newton, G. N. Effects of chain length on the size, stability, and electronic structure of redox-active organic-inorganic hybrid polyoxometalate micelles. *Mol. Syst. Des. Eng.* **2019**, *4*, 995−999.

(11) Winter, A.; Endres, P.; Schröter, E.; Jäger, M.; Görls, H.; Neumann, C.; Turchanin, A.; Schubert, U. S. Towards covalent photosensitizer-polyoxometalate dyads-bipyridyl-functionalized polyoxometalates and their transition metal complexes. *Molecules* **2019**, *24*, 4446−4466.

(12) Hampson, E.; Cameron, J. M.; Amin, S.; Kyo, J.; Watts, J. A.; Oshio, H.; Newton, G. N. Asymmetric hybrid polyoxometalates: a new platform for multifunctional redox-active nanomaterials. *Angew. Chem., Int. Ed.* **2019**, *58*, 18281−18285.

(13) Hampson, E.; Cameron, J. M.; Watts, J. A.; Newton, G. N. Transition metal decorated soft nanomaterials through modular self-assembly of an asymmetric hybrid polyoxometalate. *Chem. Commun.* **2020**, *56*, 8237−8240.

(14) Cameron, J. M.; Fujimoto, S.; Wei, R.-J.; Newton, G. N.; Oshio, H. Post-functionalization of a photoactive hybrid polyoxotungstate. *Dalton Trans.* **2018**, *47*, 10590−10594.

(15) Linnenberg, O.; Mayerl, L.; Monakhov, K. Y. The Heck reaction as a tool to expand polyoxovanadates towards thiol-sensitive organic−inorganic hybrid fluorescent switches. *Dalton Trans.* **2018**, *47*, 14402−14407.

(16) Anyushin, A. V.; Kondinski, A.; Parac-Vogt, T. N. Hybrid polyoxometalates as post-functionalization platforms: from fundamentals to emerging applications. *Chem. Soc. Rev.* **2020**, *49*, 382−432.

(17) Zhao, C.; Huang, Z.; Rodríguez-Córdoba, W.; Kambara, C. S.; O'Halloran, K. P.; Hardcastle, K. I.; Musaev, D. G.; Lian, T.; Hill, C. L. Synthesis and characterization of a metal-to-polyoxometalate charge transfer molecular chromophore. *J. Am. Chem. Soc.* **2011**, *133*, 20134−20137.

(18) Luo, Y.; Wächtler, M.; Barthelmes, K.; Winter, A.; Schubert, U. S.; Dietzek, B. Direct detection of the photoinduced charge-separated state in a Ru(II) bis(terpyridine)-polyoxometalate molecular dyad. *Chem. Commun.* **2018**, *54*, 2970−2973.

(19) Luo, Y.; Wächtler, M.; Barthelmes, K.; Winter, A.; Schubert, U. S.; Dietzek, B. Coexistence of distinct intramolecular electron transfer pathways in polyoxometalate based molecular triads. *Phys. Chem. Chem. Phys.* **2018**, *20*, 11740−11748.

(20) Matt, B.; Xiang, X.; Kaledin, A. L.; Han, N.; Moussa, J.; Amouri, H.; Alves, S.; Hill, C. L.; Lian, T.; Musaev, D. G.; Izzet, G.; Proust, A. Long lived charge separation in iridium(III)-photosensitized polyoxometalates: Synthesis, photophysical and computational studies of organometallic−redox tunable oxide assemblies. *Chem. Sci.* **2013**, *4*, 1737−1745.

(21) Black, F. A.; Jacquart, A.; Toupalas, G.; Alves, S.; Proust, A.; Clark, I. P.; Gibson, E. A.; Izzet, G. Rapid photoinduced charge injection into covalent polyoxometalate-bodipy conjugates. *Chem. Sci.* **2018**, *9*, 5578−5584.

(22) Santoni, M.-P.; Pal, A. K.; Hanan, G. S.; Tang, M.-C.; Furtos, A.; Hasenknopf, B. A light-harvesting polyoxometalate-polypyridine hybrid induces electron transfer as its Re(I) complex. *Dalton Trans.* **2014**, *43*, 6990−6993.

(23) Winter, A.; Endres, P.; Schröter, E.; Jäger, M.; Görls, H.; Neumann, C.; Turchanin, A.; Schubert, U. S. Towards covalent photosensitizer-polyoxometalate dyads-bipyridyl-functionalized polyoxometalates and their transition metal complexes. *Molecules* **2019**, *24*, 4446−4466.

(24) Luo, Y.; Maloul, S.; Schönweiz, S.; Wächtler, M.; Streb, C.; Dietzek, B. Yield-not only lifetime-of the photoinduced charge-separated state in iridium complex-polyoxometalate dyads impact their hydrogen evolution reactivity. *Chem. - Eur. J.* **2020**, *26*, 8045−8052.

(25) Allain, C.; Schaming, D.; Karakostas, N.; Erard, M.; Gisselbrecht, J.-P.; Sorgues, S.; Lampre, I.; Ruhlmann, L.; Hasenknopf, B. Synthesis, electrochemical and photophysical properties of covalently linked porphyrin-polyoxometalates. *Dalton Trans.* **2013**, *42*, 2745−2754.

(26) Santoni, M.-P.; Hanan, G. S.; Hasenknopf, B. Covalent multicomponent systems of polyoxometalates and metal complexes: Toward multi-functional organic−inorganic hybrids in molecular and material sciences. *Coord. Chem. Rev.* **2014**, *281*, 64−85.

(27) Walsh, J. J.; Bond, A. M.; Forster, R. J.; Keyes, T. E. Hybrid polyoxometalate materials for photo(electro-) chemical applications. *Coord. Chem. Rev.* **2016**, *306*, 217−234.

(28) Wu, C.; Qiao, X.; Robertson, C. M.; Higgins, S. J.; Cai, C.; Nichols, R. J.; Vezzoli, A. A chemically soldered polyoxometalate single-molecule transistor. *Angew. Chem., Int. Ed.* **2020**, *59*, 12029−12034.

(29) Dalla Francesca, K.; Lenfant, S.; Laurans, M.; Volatron, F.; Izzet, G.; Humblot, V.; Methivier, C.; Guerin, D.; Proust, A.; Vuillaume, D. Charge transport through redox active $[H_7P_8W_{48}O_{184}]^{33-}$ polyoxometalates self-assembled onto gold surfaces and gold nanodots. *Nanoscale* **2019**, *11*, 1863−1878.

(30) Pütt, R.; Qiu, X.; Kozłowski, P.; Gildenast, H.; Linnenberg, O.; Zahn, S.; Chiechi, R. C.; Monakhov, K. Y. Self-assembled monolayers of polyoxovanadates with phthalocyaninato lanthanide moieties on gold surfaces. *Chem. Commun.* **2019**, *55*, 13554−13557.

(31) Yaqub, M.; Walsh, J. J.; Keyes, T. E.; Proust, A.; Rinfray, C.; Izzet, G.; McCormac, T.; Forster, R. J. Electron transfer to covalently immobilized Keggin polyoxotungstates on gold. *Langmuir* **2014**, *30*, 4509−4516.

(32) Gumerova, N. I.; Rompel, A. Synthesis, structures and applications of electron-rich polyoxometalates. *Nature Rev. Chem.* **2018**, *2*, 1−20.

(33) Busche, C.; Vilà-Nadal, L.; Yan, J.; Miras, H. N.; Long, D.-L.; Georgiev, V. P.; Asenov, A.; Pedersen, R. H.; Gadegaard, N.; Mirza, M. M.; et al. Design and fabrication of memory devices based on nanoscale polyoxometalate clusters. *Nature* **2014**, *515*, 545−549.

(34) Vilà-Nadal, L.; Mitchell, S. G.; Markov, S.; Busche, C.; Georgiev, V.; Asenov, A.; Cronin, L. Towards polyoxometalate-cluster-based nano-electronics. *Chem. - Eur. J.* **2013**, *19*, 16502−16511.

https://dx.doi.org/10.1021/acs.inorgchem.0c02257
Inorg. Chem. XXXX, XXX, XXX−XXX

(35) Linnenberg, O.; Moors, M.; Notario-Estévez, A.; López, X.; de Graaf, C.; Peter, S.; Baeumer, C.; Waser, R.; Monakhov, K. Y. Addressing multiple resistive states of polyoxovanadates: conductivity as a function of individual molecular redox states. *J. Am. Chem. Soc.* **2018**, *140*, 16635−16640.
(36) Izzet, G.; Volatron, F.; Proust, A. Tailor−made covalent organic-inorganic polyoxometalate hybrids: Versatile platforms for the elaboration of functional molecular architectures. *Chem. Record* **2017**, *17*, 250−266.
(37) Konarev, D. V.; Kuzmin, A. V.; Khasanov, S. S.; Batov, M. S.; Otsuka, A.; Yamochi, H.; Kitagawa, H.; Lyubovskaya, R. N. Salts with titanyl and vanadyl phthalocyanine radical anions. Molecular design and effect of cations on the structure and magnetic and optical properties. *CrystEngComm* **2018**, *20*, 385−401.
(38) Glöß, M.; Pütt, R.; Moors, M.; Kentzinger, E.; Pyckhout-Hintzen, W.; Monakhov, K. Y. Interplay between the amphipathic polyoxometalate interactions in solution and at solid−liquid interfaces: A toolbox for the technical application. *Nanoscale* **2019**, *11*, 4267−4277.
(39) Linnenberg, O. *Lindqvist-Hexavanadat-basierte organisch-anorganische Hybridmaterialien als molekulare Schalter*; Verlagshaus Mainz GmbH: 2019.
(40) Finke, R. G.; Rapko, B.; Saxton, R. J.; Domaille, P. J. Trisubstituted heteropolytungstates as soluble metal oxide analogs. III. Synthesis, characterization, phosphorus-31, silicon-29, vanadium-51, and 1- and 2-D tungsten-183 NMR, deprotonation, and proton mobility studies of organic solvent solute forms of $H_xSiW_9V_3O_{40x-7}$ and $H_xP_2W_{15}V_3O_{62x-9}$. *J. Am. Chem. Soc.* **1986**, *108*, 2947−2960.
(41) Finke, R. G.; Droege, M. W.; Domaille, P. J. Trivacant heteropolytungstate derivatives. 3. Rational syntheses, characterization, two-dimensional ^{183}W NMR, and properties of $P_2W_{18}M_4(H_2O)_2O_{68}^{10-}$ and $P_4W_{30}M_4(H_2O)_2O_{112}^{16-}$ (M= Co, Cu, Zn). *Inorg. Chem.* **1987**, *26*, 3886−3896.
(42) Gerasymchuk, Y.; Tomachynski, L.; Tretyakova, I.; Hanuza, J.; Legendziewicz, J. Axially substituted ytterbium (III) monophthalocyanine - Synthesis and their spectral properties in solid state, solution and in monolithic silica blocks. *J. Photochem. Photobiol., A* **2010**, *214*, 128−134.
(43) Fukuda, T.; Kobayashi, N. In *Handbook of Porphyrin Science (Vol. 9) with Applications to Chemistry, Physics, Materials Science, Engineering, Biology and Medicine*; World Scientific: 2010; pp 1−644.
(44) Odom, B.; Hanneke, D.; D'Urso, D.; Gabrielse, G. New Measurement of the Electron Magnetic Moment Using a One-Electron Quantum Cyclotron. *Phys. Rev. Lett.* **2006**, *97*, 030801−030804.
(45) Nesmelov, Y. E.; Gopinath, A.; Thomas, D. D. Aqueous sample in an EPR cavity: Sensitivity considerations. *J. Magn. Reson.* **2004**, *167*, 138−146.
(46) Ishikawa, N. Functional phthalocyanine molecular materials. *Struct. Bonding (Berlin, Ger.)* **2010**, *135*, 211−228.
(47) Paillaud, J.; Drillon, M.; Decian, A.; Fischer, J.; Weiss, R.; Poinsot, R.; Herr, A. Organic ferromagnetic chain in the yttrium diphthalocyanine $[YPc_2]\cdot CH_2Cl_2$: X-ray structure and magnetic behavior. *Phys. B* **1991**, *175*, 337−348.
(48) Sugimoto, H.; Higashi, T.; Mori, M. Preparation and characterization of some rare-earth complexes of the phthalocyanine radical. *Chem. Lett.* **1983**, *12*, 1167−1170.
(49) Sugimoto, H.; Higashi, T.; Mori, M. Stable free radicals of phthalocyanine. *J. Chem. Soc., Chem. Commun.* **1983**, 622−623.
(50) Turek, P.; André, J.-J.; Giraudeau, A.; Simon, J. Preparation and study of a lithium phthalocyanine radical: optical and magnetic properties. *Chem. Phys. Lett.* **1987**, *134*, 471−476.
(51) Reecht, G.; Krane, N.; Lotze, C.; Franke, K. J. π-Radical formation by pyrrolic H abstraction of phthalocyanine molecules on molybdenum disulfide. *ACS Nano* **2019**, *13*, 7031−7035.
(52) Bodziony, T.; Kaczmarek, S. EPR and optical study of coupled Yb^{3+} ion pairs in weakly doped $LiNbO_3$: Yb single crystal. *Res. Chem. Intermed.* **2007**, *33*, 885.
(53) Palumbo, C. T.; Darago, L. E.; Dumas, M. T.; Ziller, J. W.; Long, J. R.; Evans, W. J. Structure, magnetism, and multi-electron reduction reactivity of the inverse sandwich reduced arene La^{2+} complex $[\{[C_5H_3(SiMe_3)_2]_2La\}_2(\mu\text{-}\eta^6\text{:}\eta^6\text{-}C_6H_6)]^{1-}$. *Organometallics* **2018**, *37*, 3322−3331.
(54) Meihaus, K. R.; Fieser, M. E.; Corbey, J. F.; Evans, W. J.; Long, J. R. Record high single-ion magnetic moments through $4f^n5d^1$ electron configurations in the divalent lanthanide complexes $[(C_5H_4SiMe_3)_3Ln]^-$. *J. Am. Chem. Soc.* **2015**, *137*, 9855−9860.
(55) Linnenberg, O.; Kozłowski, P.; Besson, C.; van Leusen, J.; Englert, U.; Monakhov, K. Y. A V_{16}-type polyoxovanadate structure with intricate electronic distribution: Insights from magnetochemistry. *Cryst. Growth Des.* **2017**, *17*, 2342−2350.
(56) Notario-Estevez, A.; Kozłowski, P.; Linnenberg, O.; de Graaf, C.; Lopez, X.; Monakhov, K. Y. Decoding the role of encapsulated ions in the electronic and magnetic properties of mixed-valence polyoxovanadate capsules $\{X@V_{22}O_{54}\}$ ($X = ClO_4^-$, SCN^-, $VO_2F_2^-$): A combined theoretical approach. *Phys. Chem. Chem. Phys.* **2018**, *20*, 17847−17858.
(57) Kozłowski, P.; Notario-Estévez, A.; de Graaf, C.; López, X.; Monakhov, K. Y. Reconciling the valence state with magnetism in mixed-valent polyoxometalates: the case of a $\{VO_2F_2@V_{22}O_{54}\}$ cluster. *Phys. Chem. Chem. Phys.* **2017**, *19*, 29767−29771.

https://dx.doi.org/10.1021/acs.inorgchem.0c02257
Inorg. Chem. XXXX, XXX, XXX−XXX